# Structure and Dynamics of Poly(*N*-isopropylacrylamide)−Clay Nanocomposite Gels

**Mitsuhiro Shibayama,*,†,‡ Junko Suda,† Takeshi Karino,†,‡ Satoshi Okabe,† Toru Takehisa,§ and Kazutoshi Haraguchi§**

*Neutron Science Laboratory, Institute for Solid State Physics, University of Tokyo, Tokai, Ibaraki 319-1106, Japan; CREST, Japan Science and Technology Agency, 4-1-8 Honcho Kawaguchi, Saitama 332-0012, Japan; and Kawamura Institute of Chemical Research, 631 Sakada, Sakura-shi, Chiba 285-0078, Japan*

*Received July 27, 2004; Revised Manuscript Received September 22, 2004*

ABSTRACT: The structure and dynamics of poly(*N*-isopropylacrylamide) (PNIPA)−clay nanocomposite (NC) gels have been investigated by small-angle neutron scattering and dynamic light scattering in order to account for their high strength and high deformability. The structure of clay dispersion in water was an assembly of clay platelets 300 Å in diameter and 10 Å thick. The structure factors of the clay dispersions were reduced to a master curve by normalizing with the clay concentration, $C_{clay}$, even across its sol−gel transition. On the other hand, the structure factors of the NC gels cannot be represented with a simple addition of the structure factors of the components, but with a sum of Lorentz (L) and squared-Lorentz (SL) functions. It was found that the SL term, indicating the gel inhomogeneities, becomes dominant by increasing $C_{clay}$. The chain dynamics of the gels was found to be similar to the conventional PNIPA gels chemically cross-linked with bis-acrylamide.

## Introduction

Recently, clay−polymer nanocomposites have been focused much attention because of their excellent physical properties, such as toughness, high modulus, heat resistance, transparency, and so on.[1,2] These properties are much superior to those expected by a simple additive rule. This is partially due to strong interactions at the clay−polymer interface. Owing to the nature of complex molecules of clay, chemical reactivity is high at the clay surface, which allows a variety of chemical reaction at the surface including complex chemistry.[3,4] In addition, clay molecules often have quite a large aspect ratio, such as narrow rods or thin platelets. These unique shapes of clay are very suitable as a reinforcing filler of polymer materials. As a result, a variety of engineering plastics have been proposed and commercialized, e.g., polyamide−clay nanocomposites.[4]

Haraguchi et al. reported a novel clay−polymer nanocomposite gels (NC gels) consisting of synthetic hectorite and poly(*N*-isopropylacrylamide) (PNIPA). This "nanocomposite hydogel" (after their notation) has excellent physical properties, such as tough mechanical properties, large deformability, large swelling ratio, rapid shrinking capability, and high transparency.[5,6] This clay is typically used in clay−polymer nanocomposites and has a shape of a platelet 300 Å in diameter and 10 Å in thickness. The plane surface and edge are charged to be negative and positive, respectively. On the other hand, PNIPA is known to be a temperature-sensitive polymer in aqueous media. It undergoes thermoreversible phase separation around 32 °C.[7−9] Hydrogels made of PNIPA shrinks or swells across this temperature. Since PNIPA gels are fragile, they are not suitable for most of applications. The clay−PNIPA nanocomposite hydrogels, however, are much tougher and deformable by a factor of 20−50 in deformability and of 300−1000 in toughness in comparison with conventional PNIPA hydrogels.

The purpose of this work is to elucidate the molecular origin of the excellent physical properties of the NC hydrogels from the structure and molecular dynamics points of view. Here, we employ small-angle neutron scattering (SANS), X-ray scattering (SAXS), and dynamic light scattering (DLS) and unveil the unique structure/dynamics of NC gels as a function of clay concentration.

## Experimental Section

**Samples.** *N*-isopropylacrylamide (NIPA) monomer (Kohjin Co., Ltd., Japan) was purified by recrystallization from a toluene/*n*-hexane mixture, followed by drying in vacuo. As an inorganic clay, synthetic hectorite "Laponite XLG" (Rockwood Ltd.), $[Mg_{5.34}Li_{0.66}Si_8O_{20}(OH)_4]Na_{0.66}$, was used. The purified monomer was dissolved in deionized water (or $D_2O$) containing dispersion of the inorganic clay. Prior to dissolution, oxygen in the deionized water (or $D_2O$) was removed by bubbling $N_2$ gas for more than 3 h. Potassium peroxodisulfate and *N*,*N*,*N*′,*N*′-tetramethylethylenediamine (TEMED) were used as an initiator and catalyst, respectively. The molar ratio of the monomer, initiator, and catalyst was 100:0.426:0.735. Redox polymerization was carried out at 20 °C for 20 h. Thus, prepared gels were used for scattering experiments without further treatment. The NIPA concentration was kept to be 7.8 wt %, and the clay concentration was varied as shown in Table 1. The sample code is defined by the ratio of the clay and water, e.g., clay(1.0) and NC(1.0), indicating 0.01 mol of clay (= 7.62 g) in 1 L of $H_2O$ or $D_2O$ for the clay dispersion and NC gel, respectively. Thus, clay(0.05) to clay(4.0) and NC(0.0) to NC-(4.0) were prepared.

**Small-Angle Neutron Scattering (SANS).** SANS experiments were performed at the two-dimensional SANS instrument (SANS-U), Neutron Science Laboratory, the University of Tokyo, installed at Japan Atomic Energy Research Institute, Tokai, Japan. The neutron wavelength was 7.0 Å. The monochromatization was attained with a mechanical velocity selector, and the wavelength distribution was ca. 13%. The samples

† University of Tokyo.
‡ CREST, Japan Science and Technology Agency.
§ Kawamura Institute of Chemical Research.
* To whom corresponding should be addressed. E-mail sibayama@issp.u-tokyo.ac.jp.

10.1021/ma048464v CCC: $27.50 
Published on Web 11/13/2004

**Table 1. Samples**

| $C_{clay}$/wt % | $C_{clay}$/($10^{-2}$ mol/L) | clay dispersion | NC gel |
|---|---|---|---|
| 0 | 0.0 | | NC(0.0) |
| 0.0381 | 0.05 | clay(0.05) | NC(0.05) |
| 0.0762 | 0.1 | clay(0.1) | NC(0.1) |
| 0.191 | 0.25 | | NC(0.25) |
| 0.381 | 0.5 | clay(0.5) | NC(0.5) |
| 0.762 | 1.0 | clay(1.0) | NC(1.0) |
| 1.52 | 2.0 | | NC(2.0) |
| 3.05 | 4.0 | clay(4.0) | NC(4.0) |

of clay dispersion and NC gels were filled in a quartz cell and irradiated with the monochromatized neutron beam for 30−120 min, depending on the scattering intensity counts. The sample-to-detector distance was 2, 4, and 8 m, depending on the experimental conditions. The scattered neutrons were collected with a two-dimensional detector (model 2660N, Ordela) and then were circularly averaged before necessary corrections, such as air scattering and cell scattering. After these corrections, the scattered intensity was normalized to the absolute intensity, i.e., the differential cross section in terms of scattering intensity from a standard sample. The incoherent scattering correction was made by subtracting the scattering intensity from a NIPA monomer in $D_2O$ solution. The temperature of the samples was regulated to be 20 °C with a water-circulating bath controlled with a Neslab RTE-111 thermocontroller with the precision of ±0.1 °C.

**Static/Dynamic Light Scattering (SLS/DLS).** SLS/DLS experiments were carried out with an ALV5000 static/dynamic spectrometer (ALV, Langen, Germany). The light source was a 22 mW He−Ne laser. A combination of a static and dynamic enhancer was installed to gain the signal-to-noise ratio. The intensity−time correlation function, $g^{(2)}(\tau)$, was obtained as a function of the decay time, $\tau$, at 20 °C and at various scattering angles. A typical sampling time was 30 s.

**Small-Angle X-ray Scattering (SAXS).** Supplemental SAXS experiments were also carried out with a Rigaku RU1800 coupled with a focusing device (NanoViewer) and an imaging plate. The wavelength of the X-ray was 1.54 Å, operated at 40 kV and 20 mA. The typical exposure time was 30 min. The beam size was 0.4 mm diameter. The sample-to-detector distance was 550 mm.

## Results and Discussion

**1. Structure Factors of Clay Dispersions and NC Gels**. Figure 1a shows SANS intensity functions, $I(q)$s, of clay dispersion in $D_2O$. The $I(q)$ increases with increasing clay concentration, $C_{clay}$. However, they seem to be superimposed by normalizing with $C_{clay}$, as shown in Figure 1b. Note that the clay dispersions were in sol state for clay(2.0) and below within the time range of the experiments, while clay(4.0) was in gel state. Hence, the structure factors of clay dispersion do not change by sol−gel transition. This indicates that clay platelets form a self-similar aggregate structure irrespective of its concentration, and the sol−gel transition is nothing but a volume-filling phenomenon of the clay aggregates.

The structure of clay dispersion can be discussed by SANS experiments. Figure 2 shows the result of curve fitting for clay(4.0) with a scattering function, $P(q)$, for a randomly oriented platelet with thickness $2H$ and the radius $R$ given by

$$P(q) = \int_0^{\pi/2}\left\{\frac{2J_1(qR\sin\alpha)}{qR\sin\alpha}\frac{\sin(qH\cos\alpha)}{qH\cos\alpha}\right\}^2 \sin\alpha\, d\alpha \sim \int_0^{\pi/2}\left\{\frac{2J_1(qR\sin\alpha)}{qR\sin\alpha}\right\}^2 \sin\alpha\, d\alpha \quad (1)$$

where α is the polar angle with respect to the direction along the platelet normal and $J_1(x)$ is the Bessel function

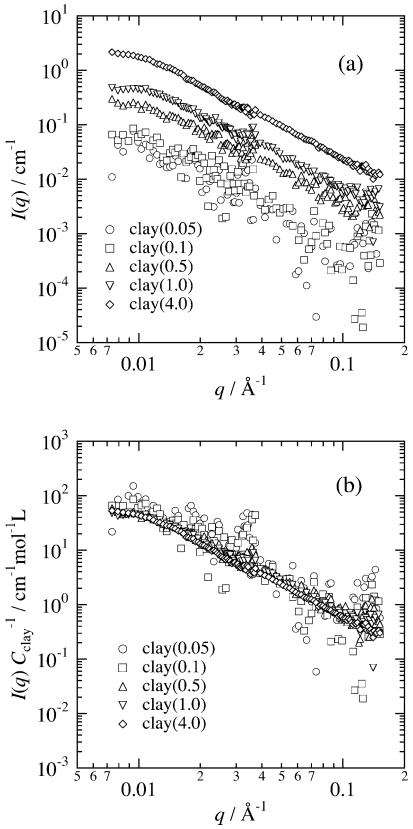


**Figure 1.** SANS intensity curves for (a) clay dispersions in $D_2O$ having different clay concentrations, $C_{clay}$s, and (b) their master curve normalized with $C_{clay}$. The numbers in the parentheses denote the clay concentrations in $10^{-2}$ mol/L.

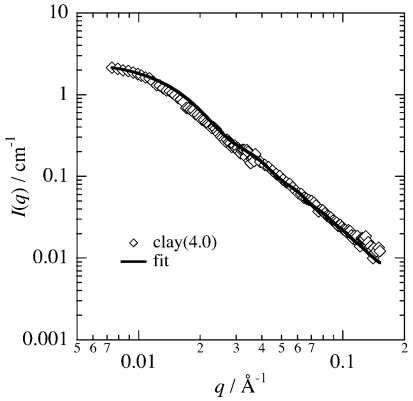


**Figure 2.** SANS intensity function of clay(4.0) and the result of curve fit with eq 1.

of the order of 1. As shown by the solid line, the observed $I(q)$ is well reproduced with eq 1. The parameters used for the fitting were $2R \approx 300$ Å and $2H \approx 10$ Å, which are in good agreement with the literature values for hectorite platelets.[10]

To discuss the structure factor, however, it is more convenient to employ the following function. Equation 2 is a scattering function consisting of Lorentz (L) and squared-Lorentz (SL) functions, i.e.[11,12]

$$I(q) = \frac{I_L(0)}{1+q^2\xi^2} + \frac{I_{SL}(0)}{(1+q^2\Xi^2)^2} \quad (2)$$

where $\xi$ is the correlation length and $\Xi$ is the characteristic length representing inhomogeneities. The L function is the same as the so-called Ornstein−Zernike

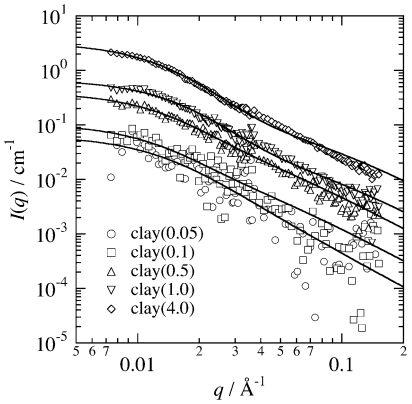


**Figure 3.** SANS intensity functions of clay dispersions in $D_2O$ having different $C_{clay}$s and the results of curve fitting with eq 2, i.e., the Lorentz and squared-Lorentz functions.

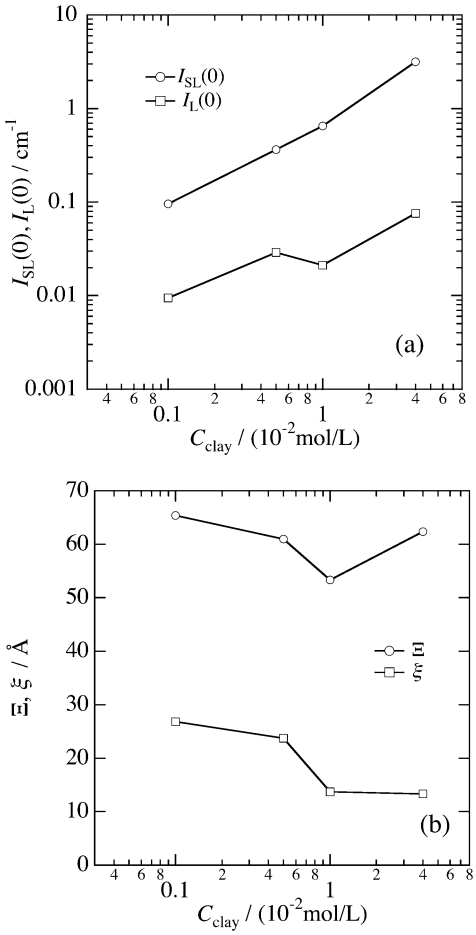


**Figure 4.** $C_{clay}$ dependence of the fitting parameters for the clay dispersions: (a) $I_{SL}(0)$ and $I_L(0)$; (b) $\Xi$ and $\xi$.

function and is well-known to describe the structure factor of polymer solutions in semidilute regime.[13] On the other hand, the SL function is often introduced to describe the cross-link inhomogeneities.[11] Figure 3 shows the result of curve fitting for the clay dispersions with eq 2. As shown in the figure, the fitting is satisfactory.

Figure 4 shows the variation of the fitting parameters, i.e., (a) $I_L(0)$ and $I_{SL}(0)$ and (b) $\xi$ and $\Xi$, with $C_{clay}$. Since $I_{SL}(0)$ increases rather linearly with $C_{clay}$, the structure factor of the clay dispersions is mainly described by the SL function. The values of $\xi$ and $\Xi$ do not depend on $C_{clay}$, indicating that the structure of the clay dispersions

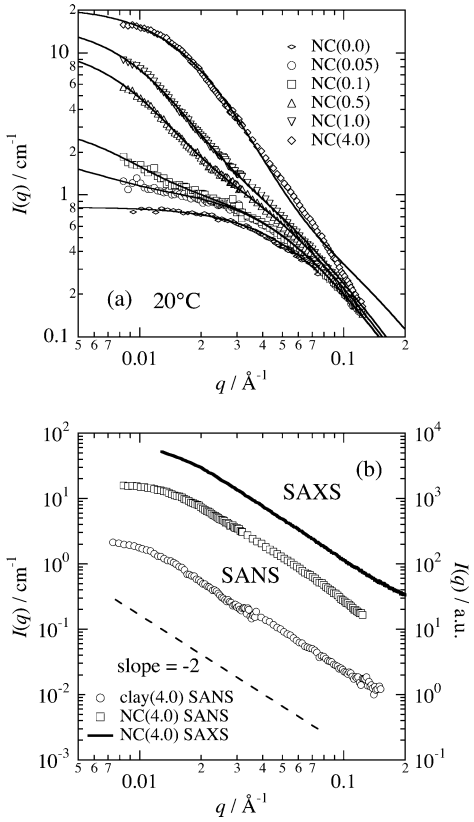


**Figure 5.** (a) SANS intensity functions of NC gels at 20 °C. The solid lines are the fits with eq 2. (b) Comparison of the SANS intensity functions for clay dispersion, clay(4.0) and NC gel, NC(4.0), and SAXS intensity function for NC(4.0). The dashed line indicates the slope of −2.

is essentially the same irrespective of $C_{clay}$. In addition, a phenomenological relationship, i.e., $\Xi = 60$ Å is equivalent to $R = 150$ Å and $\xi \approx 2H$, may be drawn.

Figure 5a shows SANS intensity functions of NC gels, i.e., clay and PNIPA nanocomposite gels. Different from the case of the clay dispersions shown in Figure 1, the shapes of $I(q)$s change with increasing with $C_{clay}$. As shown in the figure, $I(q)$s of NC gels are much larger than those of the corresponding clay dispersions. Therefore, the following conclusion can be drawn from the experimental result on the structure factor of NC gels and their precursors. NC(0.0), i.e., PNIPA solution, exhibits a SANS function similar to a polymer solution in a semidilute regime. Hence, $I(q)$ can be represented by a Lorentz function, i.e.[13]

$$I(q) = I_{PNIPA}(q) \equiv \frac{I(0)}{1 + \xi^2 q^2} \tag{3}$$

The value of $\xi$ for NC(0.0) is evaluated to be 18 Å, which is in good agreement with the literature values.[14] By increasing $C_{clay}$, $I(q)$ increases at the low $q$ region. Note that the system instantaneously becomes gels in the presence of clay in the system. The solid lines in Figure 5a show the results of curve fitting of the scattering functions of NC gels with eq 2. As shown in the figure, the observed intensity functions are well reproduced by eq 2.

Figure 5b shows the SANS intensity functions of NC-(4.0) (squares) and clay(4.0) (circles) and SAXS intensity of NC(4.0) (solid line). As shown in the figure, $I(q)$s of NC(4.0) obtained by SANS and SAXS seem to be well superimposed with that of clay(4.0), and their asymptote

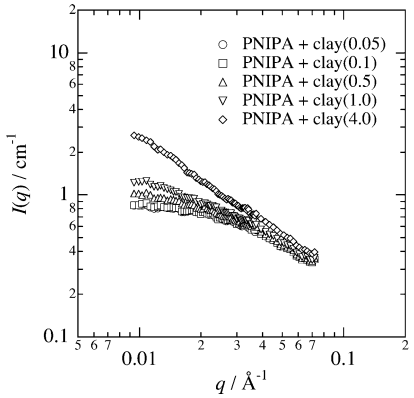


**Figure 6.** Calculated SANS intensity functions with the assumption of simple additivity.

is given by a function of slope −2 in the log−log plot (dashed line). It should be noted that SAXS data were also taken for NC(2.0) and NC(6.0), and the scattering shoulder in $I(q)$ shifts systematically toward the high $q$ region with increasing clay concentration. This may suggest that the peak indicates the interclay distance, and the distance decreases with increasing the clay concentration. This experimental observation indicates that the clay structure is more effectively observed by SAXS than by SANS. This result is quite reasonable. The neutron scattering length densities, $\rho$, are calculated to be $\rho_{clay} = 39.2 \times 10^9$ cm$^{-2}$, and $\rho_{PNIPA} = 9.33 \times 10^9$ cm$^{-2}$, and $\rho_{D_2O} = 63.4 \times 10^9$ cm$^{-2}$ with the observed mass densities $d_{clay} = 2.65$ g/cm$^3$ and $d_{PNIPA} = 1.26$ g/cm$^3$. Since the difference in $\rho$'s between PNIPA and $D_2O$ is larger than that between clay and $D_2O$, the PNIPA chain conformation is selectively observed by SANS. On the other hand, the electron densities, $\rho_e$, are also calculated to be $\rho_{e,clay} = 7.98 \times 10^{23}$ electrons/cm$^3$, $\rho_{e,PNIPA} = 4.16 \times 10^{23}$ electrons/cm$^3$, and $\rho_{e,H_2O} = 3.34 \times 10^{23}$ electrons/cm$^3$. These values indicate that SAXS is much more sensitive to clay than PNIPA chains. As a result, it can be concluded that SANS and SAXS are complimentary and detect the PNIPA network structure and clay structure, respectively.

Figure 6 show the calculated scattering intensity by assuming a simple additivity

$$I_{calc}(q) = I_{clay}(q;C_{clay}) + I_{PNIPA}(q) \quad (4)$$

where $I_{clay}(q;C_{clay})$ is the structure factor of clay dispersion with the clay concentration of $C_{clay}$, and $I_{PNIPA}(q)$ is that of PNIPA solution. Comparison of Figures 5a and 6 suggests that the structure factor of NC gels cannot be given by a simple addition of the scattering functions of the components. Lal and Auvray reported that a simple additive rule on the SANS intensity could not be applied for a mixture of poly(ethylene oxide) (PEO) and Laponite clay in $D_2O$.[15] The scattering intensities of the clay and PEO solutions were scaled to $q^{-2}$ and $q^{-1.58}$, respectively, and the scattering intensity from a mixture was much stronger than either of them and was scaled to $q^{-2}$. They conjectured that the Laponite surface was decorated by PEO chains. In the case of NC gels, not only surface deposition but also chain anchoring must be present because NIPA monomer is polymerized in the atmosphere of clay dispersion. This must be why extraordinarily strong mechanical properties are generated.

Figure 7a,b shows the results of curve fitting shown in Figure 5a. As expected, $I_{SL}(0)$ increases rather

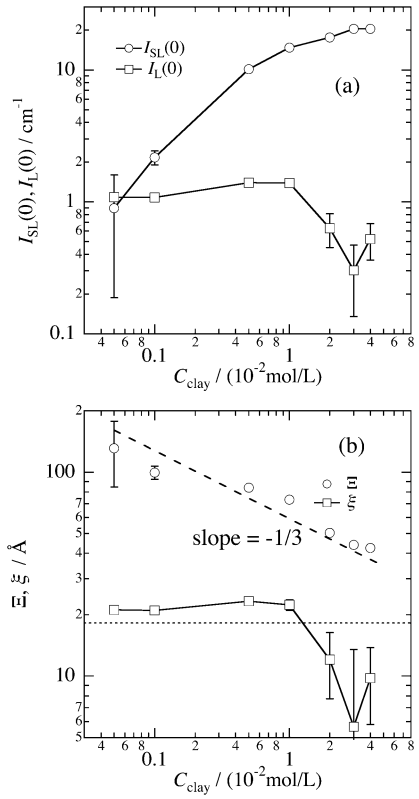


**Figure 7.** $C_{clay}$ dependence of the fitting parameters for the NC gels: (a) $I_{SL}(0)$ and $I_L(0)$; (b) $\Xi$ and $\xi$. The horizontal dotted line indicates the value of PNIPA solution at 20 °C, and the dashed line denotes the slope of −1/3.

linearly with $C_{clay}$, while $I_L(0)$ remains constant. This result suggests the SL term is the leading term to represent the structure of NC gels. In Figure 7b is shown the correlation length, $\xi$, for the NC gels (the horizontal dotted line) is very close to that of PNIPA gel, and $I_L(0)$ is rather independent of $C_{clay}$. This fact is quite reasonable since the PNIPA concentration is the same for all of the samples studied here. It is quite interesting to note that $\Xi$ decreases with $C_{clay}^{-1/3}$ as shown by the dashed line in Figure 7b. This indicates that $\Xi$ means the interplatelet distance and the clay platelets randomly dispersed in a three-dimensional space, and the interplatelet distance decreases with increasing the platelet concentration, $C_{clay}$.

To investigate the spatial inhomogeneities, static light scattering (SLS) experiment was also carried out. Figure 8 shows the plots of scattering intensity variation in both the LS ($0.0006 \le q \le 0.002$ Å$^{-1}$) and SANS regions ($0.007 \le q \le 0.1$ Å$^{-1}$). The scattering contrasts for LS and SANS, $K_{LS}$ and $K_{SANS}$, were evaluated with the following equations:[16]

$$K_{LS} = \frac{2\pi^4 n_0^2 \left(\frac{\partial n}{\partial c}\right)^2}{N_A \lambda_0^4} = 9.63 \times 10^{-7} \text{ [mol cm}^2\text{/g}^2\text{]} \quad (5)$$

$$K_{SANS} = \left(b_p - b_0\left(\frac{v_p}{v_0}\right)\right)^2 \frac{N_A}{M_m^2} = 4.19 \times 10^{-3} \text{ [mol cm}^2\text{/g}^2\text{]} \quad (6)$$

where $N_A$ is the Avogadro's number, $n_0$ is the refractive index of the solvent (i.e., water), d$n$/d$c$ is the refractive index increment with respect to the solute concentra-

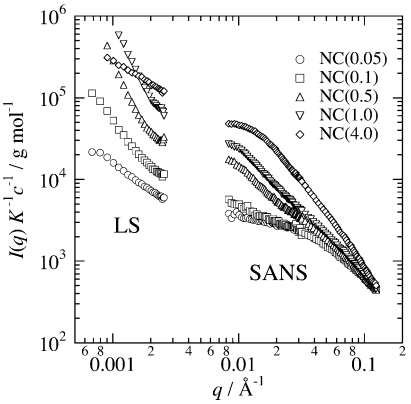


**Figure 8.** Wide range scattering intensity functions obtained by light scattering and small-angle neutron scattering. The intensities were scaled to the absolute intensities by using eq 5 and 6.

tion, $c$, $b_p$ and $b_0$ are the scattering lengths of the polymer (PNIPA) and the solvent (water), $v_p$ and $v_0$ are the monomer volume of the polymer and solvent, and $M_m$ is the molecular weight of the solute. Figure 8 shows that the scattering intensity functions obtained by LS and SANS are well connected without ambiguity. It should be noted that $I(q)$s from NC(1.0) to NC(4.0) show a crossover in the LS regime. That is, the scattering intensity of NC(0.5) and NC(1.0) are larger than that of NC(4.0) for $q \leq 0.0015$ Å$^{-1}$. This phenomenon suggests that percolation transition takes place in the clay concentration range of $1.0 \leq C_{clay} \approx 4.0$ ($\times 10^{-2}$ mol/L). Note that turbidity becomes largest at the percolation transition, similar to critical opalescence in the vapor-to-liquid transition.[17,18]

**2. Dynamics of Clay Dispersions and NC Gels.** Figure 9 shows time−intensity correlation functions of (a) clay dispersions and (b) NC gels. The time−intensity correlation function, $g^{(2)}(\tau)$, is defined by

$$g^{(2)}(\tau) = \frac{\langle I(t)I(t+\tau)\rangle}{\langle I(t)\rangle^2} \tag{7}$$

Interestingly, $g^{(2)}(\tau)$s of clay dispersions are roughly the same for clay(0.05), clay(0.1), clay(0.5), and clay(1.0) irrespective of $C_{clay}$. On the other hand, $g^{(2)}(\tau)$ of clay-(4.0) is quite different. These features agree with the fact that sol−gel transition takes place between the two concentrations. In the case of NC gels, $g^{(2)}(\tau)$ has a characteristic decay time around $10^{-1}$ ms. This corresponds to the so-called gel mode in chemical gels, meaning the collective motion of the subchains in polymer networks.[19]

Figure 10 shows the decay rate distribution functions, $G(\Gamma)$s, for (a) clay dispersions and (b) NC gels obtained by an inverse Laplace transform of $g^{(2)}(\tau)$ with the so-called CONTIN algorithm, i.e.

$$g^{(2)}(\tau) - 1 = [\int_0^\infty G(\Gamma)\exp(-\Gamma\tau)\,d\Gamma]^2 \tag{8}$$

Each of $G(\Gamma)$s for the clay dispersions has a single peak, which is decreasing and shifting toward the larger relaxation time with $C_{clay}$. A broadening of $G(\Gamma)$ took place between clay(1.0) and clay(4.0) as a result of sol−gel transition. For clay(1.0) and less, the mode was translational and diffusive, while a slow relaxation mode appeared. This behavior was in good agreement with the result reported by Kroon et al.[20] In the case of NC

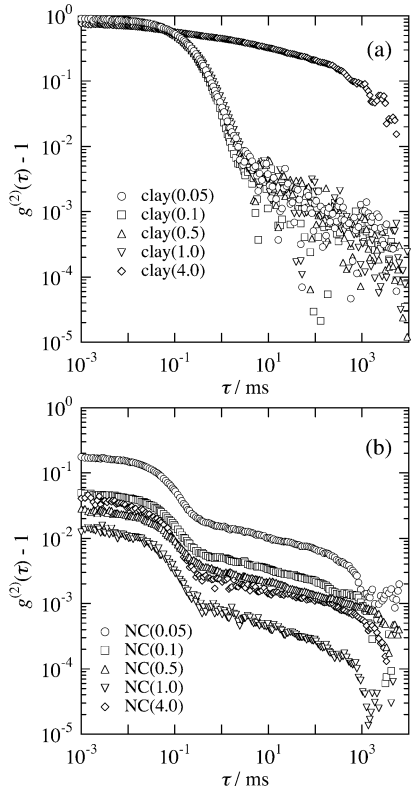


**Figure 9.** Time−intensity correlation functions, $g^{(2)}(\tau)$, for (a) clay dispersions and (b) NC gels.

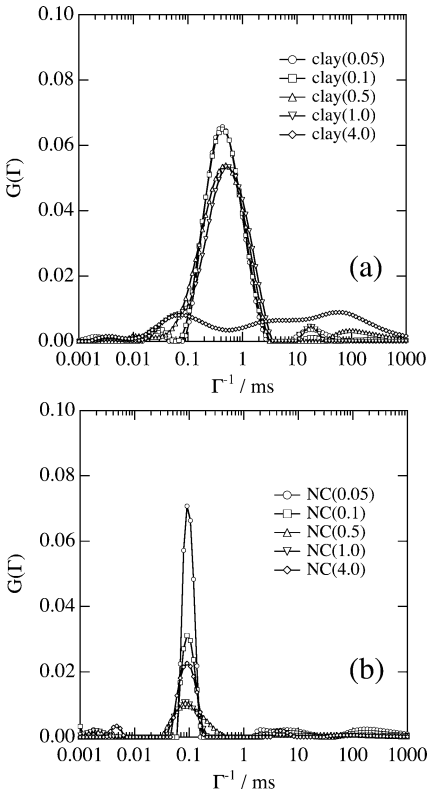


**Figure 10.** Decay rate distribution functions, $G(\Gamma)$s, for (a) clay dispersions and (b) NC gels.

gels, $G(\Gamma)$s have much sharper peaks. This clearly shows that the origin of the relaxation process between clay and NC gels are very different. That is, the former is the translational diffusion of clay platelets, while the latter is the collective diffusion of gel network.[21,22] In general, the collective diffusion of polymer gels give a

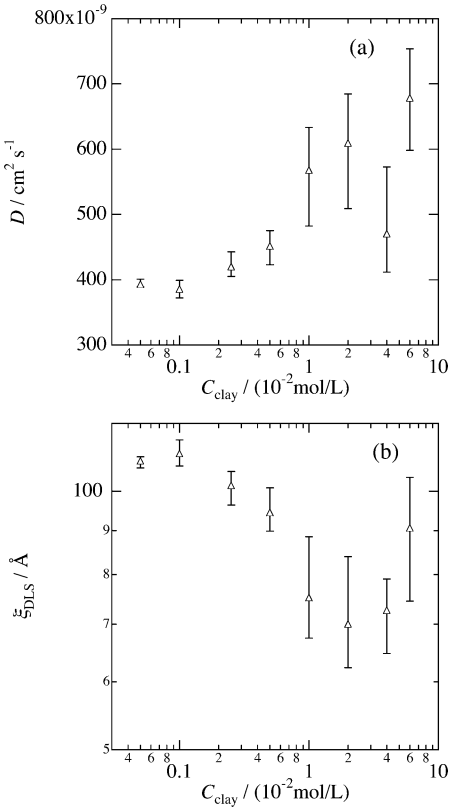


**Figure 11.** Variations of (a) the collective diffusion coefficient, $D$, and (b) the correlation length obtained by DLS, $\xi_{DLS}$.

very sharp peak in $G(\Gamma)$ compared to the translational diffusion mode of individual chains.[23] Although the peak for NC(4.0) is larger than those for NC(0.5) and NC-(1.0), this is simply due to the nonergodicity of gels.

Figure 11 shows $C_{clay}$ dependence of (a) collective diffusion coefficient, $D$, and (b) the correlation length, $\xi_{DLS}$, where $\xi_{DLS}$ is evaluated by[21]

$$\xi_{DLS} \approx \frac{kT}{6\pi\eta D} \tag{9}$$

To account for the nonergodicity of gels, nominal values of diffusion coefficient, $D_A$, were evaluated at a hundred different sample positions with

$$D_A = -\frac{1}{2q^2}\lim\frac{\partial}{\partial\tau}\ln[g^{(2)}(\tau) - 1] \tag{10}$$

and then $D_A$ was extrapolated to the pure-homodyne limit to obtain the collective diffusion coefficient, $D$. The details of evaluation method is described elsewhere.[24] Here, $q$ is the magnitude of the scattering vector of the incident light. $\xi_{DLS}$ is a decreasing function with $C_{clay}$. This indicates that mesh size decreases with $C_{clay}$.

Figure 12 shows clay concentration dependence of the correlation lengths, $\xi$, $\xi_{DLS}$, and $\Xi$. Interestingly, $\xi_{DLS}$ and $\Xi$ are roughly the same with respect not only to the $C_{clay}$ dependence but also to their values. On the other hand, the value of $\xi$ is much smaller than the others. A disagreement of $\xi$ and $\xi_{DLS}$ has been often pointed out in the literature.[25] This is simply due to the missing of the scaling factor in eq 9. However, the agreement of $\xi_{DLS}$ and $\Xi$ means that the dynamic fluctuations ($\xi_{DLS}$) can be also detectable by SANS as the characteristic length of inhomogeities ($\Xi$). Particularly, the physical meaning of $\Xi$ is deduced to be the

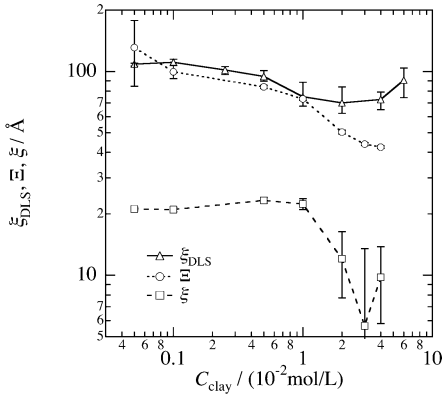


**Figure 12.** Comparison of the variations of $\Xi$, $\xi$ , and $\xi_{DLS}$ with $C_{clay}$.

interplatelet distance at least in this system. This fact may propose a new interpretation about the gel inhomogeneities since the correlation length obtained from the SL component has been believed to represent not dynamic concentration fluctuations but frozen concentration fluctuations.[11,24,26] Further investigations along this line are in progress.

## Conclusion

The structure and dynamics of PNIPA−clay nanocomposite gels have been investigated in terms of SANS, DLS, and SAXS. The following facts were disclosed. (1) $I(q)$s for clay dispersions can be reduced with $C_{clay}$, indicating a self-similar structure irrespective of $C_{clay}$. The structure factor is independent of sol−gel transition. Hence, the sol−gel transition of clay dispersion simply means a percolation threshold. The curve fitting suggests the presence of noncorrelated randomly oriented clay platelets of 300 Å diameter and 10 Å thickness. (2) $I(q)$s for NC gels cannot be described by a simple addition of the scattering functions of the components, i.e., the scattering intensities from clay dispersions and PNIPA solutions. This indicates that the structure of NC gels is very different from the clay or PNIPA solutions, and PNIPA chains are anchored to the clay platelets and decorate them with an excess monomer density near the platelet surface. The structure factor for the NC gels is well reproduced with a scattering function consisting of Lorentz and squared-Lorentz functions. The former represents the PNIPA solutions, and the latter accounts for the cross-link inhomogeneities. (3) DLS was found to be sensitive to the sol−gel transition. The mesh size, $\xi_{DLS}$, partitioned by the platelets decreases with $C_{clay}$, which was in good accordance with the variation of $\Xi$ with $C_{clay}$.

**Acknowledgment.** This work is partially supported by the Ministry of Education, Science, Sports and Culture, Japan (Grant-in-Aid 16350120). The SANS experiment was performed with the approval of Institute for Solid State Physics, The University of Tokyo (Proposal No. 04-4539), at Japan Atomic Energy Research Institute, Tokai, Japan. The authors are grateful to Rigaku Corp., Tokyo, for the kindness to use the SAXS instrument (Nano Viewer).

## References and Notes

(1) Schmidt, H. In *Materials Research Society*; Schaefer, D. W., Mark, J. E., Eds.: Elsevier: New York, 1990; p 3.
(2) Novak, B. M. *Adv. Mater.* **1993**, *5*, 422.

(3) van Olphen, H. *Clay Colloid Chemistry*, 2nd ed.; John Wiley: New York, 1977.
(4) Pinnavaia, T. J.; Beall, G. W. *Polymer-Clay Nanocomposites*: Chichester, 2000.
(5) Haraguchi, K.; Takeshita, T. *Adv. Mater.* **2002**, *14*, 1121.
(6) Haraguchi, K.; Takeshita, T.; Fan, S. *Macromolecules* **2002**, *35*, 10162.
(7) Hirokawa, Y.; Tanaka, T. *J. Chem. Phys.* **1984**, *81*, 6379.
(8) Schild, H. G. *Prog. Polym. Sci.* **1992**, *17*, 163.
(9) Shibayama, M.; Tanaka, T. *Adv. Polym. Sci.* **1993**, *109*, 1.
(10) Saunders, J. M.; Goodwin, J. W.; Richardson, R. M.; Vincent, B. *J. Phys. Chem. B* **1999**, *103*, 9211.
(11) Onuki, A. *J. Phys. II* **1992**, *2*, 45.
(12) Shibayama, M.; Isono, K.; Okabe, S.; Karino, T.; Nagao, M. *Macromolecules* **2004**, *37*, 2909.
(13) de Gennes, P. G. *Scaling Concepts in Polymer Physics*; Cornell University: Ithaca, NY, 1979.
(14) Norisuye, T.; Kida, Y.; Masui, N.; Tran-Cong-Miyata, Q.; Maekawa, Y.; Yoshida, M.; Shibayama, M. *Macromolecules* **2003**, *36*, 6202.
(15) Lal, J.; Auvray, L. *J. Appl. Crystallogr.* **2000**, *33*, 673.
(16) Shibayama, M.; Norisuye, T.; Ikkai, F. *J. Phys. Soc. Jpn., Suppl. A* **2001**, *70*, 306.
(17) Norisuye, T.; Shibayama, M.; Nomura, S. *Polymer* **1998**, *39*, 2769.
(18) Shibayama, M.; Norisuye, T. *Bull. Chem. Soc. Jpn.* **2002**, *75*, 641.
(19) Tanaka, T.; Hocker, L. O.; Benedek, G. B. *J. Chem. Phys.* **1973**, *59*, 5151.
(20) Kroon, M.; Wegdam, G. H.; Sprik, R. *Phys. Rev. E* **1996**, *54*, 6541.
(21) Tanaka, T. In *Dynamic Light Scattering*; Pecora, R., Ed.; Plenum Publishing: New York, 1985; p 347.
(22) Shibayama, M.; Isaka, Y.; Shiwa, Y. *Macromolecules* **1999**, *32*, 7086.
(23) Takeda, M.; Norisuye, T.; Shibayama, M. *Macromolecules* **2000**, *33*, 2909.
(24) Shibayama, M. *Macromol. Chem. Phys.* **1998**, *199*, 1.
(25) Shibayama, M.; Tanaka, T.; Han, C. C. *J. Chem. Phys.* **1992**, *97*, 6829.
(26) Hecht, A. M.; Duplessix, R.; Geissler, E. *Macromolecules* **1985**, *18*, 2167.

MA048464V